Electronic Supplementary Information

Triboelectric Junction:
A Model for Dynamic Metal-semiconductor Contacts

Xiaote Xu,[ab] Zhong Lin Wang*[cd] and Zhengbao Yang*[ab]

[a] Department of Mechanical and Aerospace Engineering, Hong Kong University of Science and Technology, Clear Water Bay, Hong Kong, China
[b] Department of Mechanical Engineering, City University of Hong Kong, Hong Kong, China
[c] Beijing Institute of Nanoenergy and Nanosystems, Chinese Academy of Sciences, Beijing, 101400, People's Republic of China
[d] School of Materials Science and Engineering, Georgia Institute of Technology, Atlanta, GA, 30332, USA

Email: zbyang@ust.hk; zhong.wang@mse.gatech.edu

This file includes:

Supplementary Figures

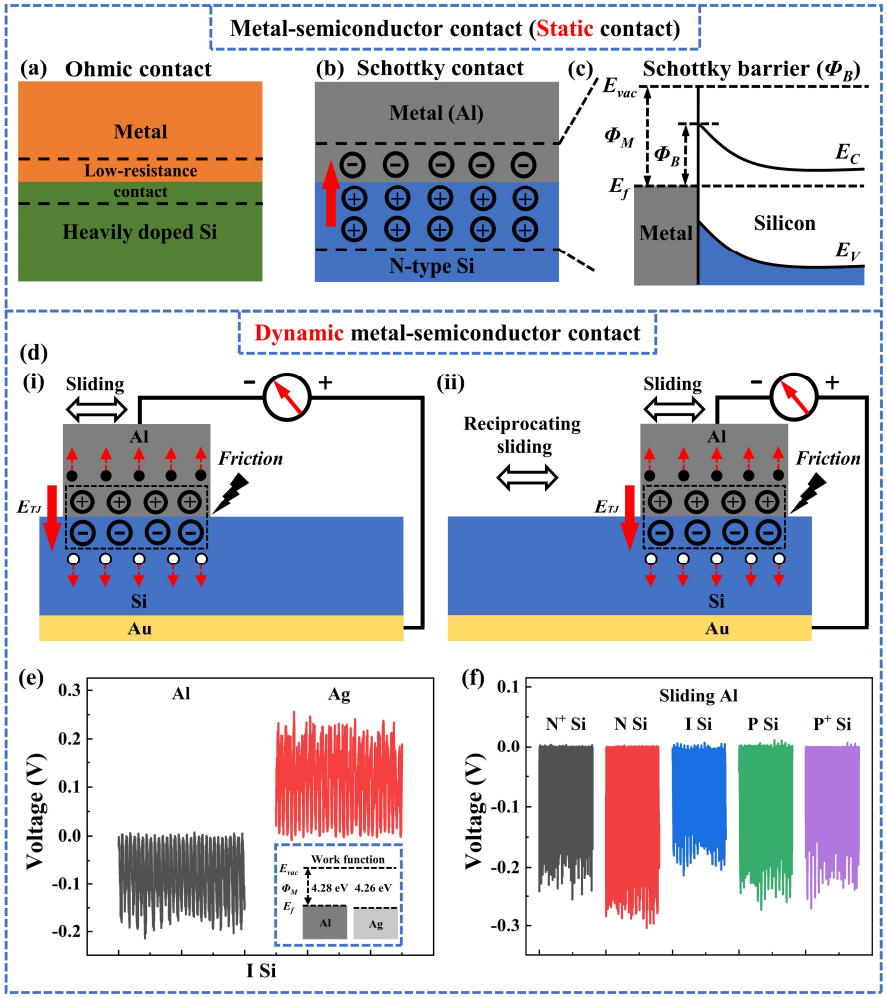

Figure S1. Metal-semiconductor contacts. (a) Schematic diagram of an Ohmic contact; and (b) Schottky contact; (c) Schottky barrier model; (d) The reciprocating sliding of a dynamic semiconductor generator; (e-f) Output characteristics in dynamic metal-semiconductor contacts that cannot be sufficiently explained by the Schottky junction theory: (e) Al and Ag have similar work-function values of about 4.28 eV and 4.26 eV, respectively, which should form similar Schottky barrier heights when contacting the same silicon. However, the output polarity of a dynamic Al-Si contact is opposite to that of a dynamic Ag-Si contact; (f) The output polarity remains consistent when sliding the same metal material on silicon wafers with different Fermi levels. However, according to the Schottky junction theory, those Ohmic contacts should not generate electric outputs, especially when using heavily doped silicon.

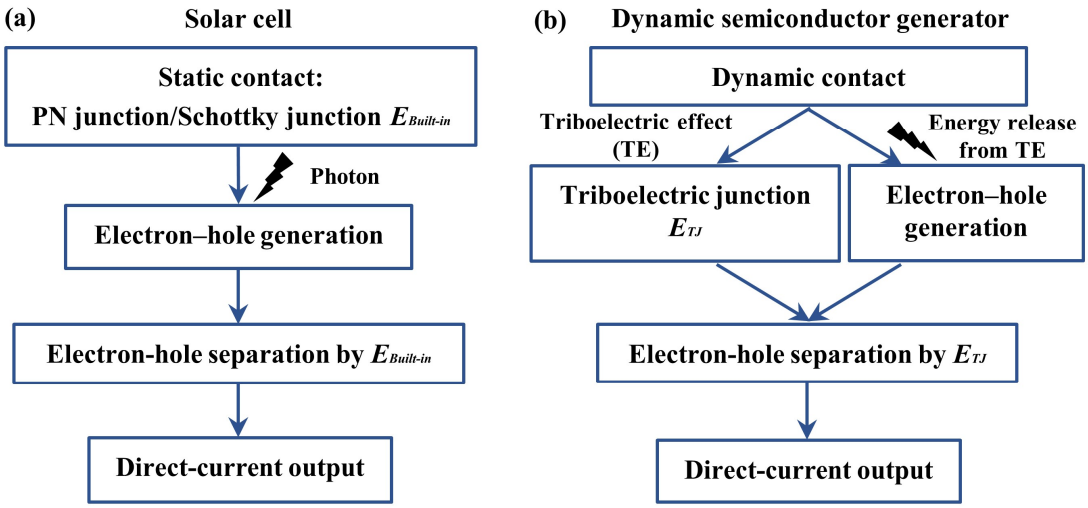

Figure S2. Comparison of the working mechanism between a solar cell and a dynamic semiconductor generator. (a) Solar cell; (b) Dynamic semiconductor generator. The working mechanism of a dynamic semiconductor generator shares similarities with a solar cell. Both involve a junction region (space charge region) that drives electron-hole separation to generate direct-current output. However, there are some significant differences between them: 1) Mechanism of junction formation: The triboelectric junction in a dynamic semiconductor generator is induced by the triboelectric effect, which only exists in dynamic contacts, while the PN junction or Schottky junction (static contacts) in a solar cell is formed due to the alignment of Fermi levels. 2) Mechanism of the non-equilibrium electron-hole generation: Photons carrying energy greater than the semiconductor bandgap excite the electron-hole generation in a solar cell; however, the excitation energy for the electron-hole generation in a dynamic semiconductor generator is from the contact-electrification, likely the released energy from the formation of a chemical bond[1,2].

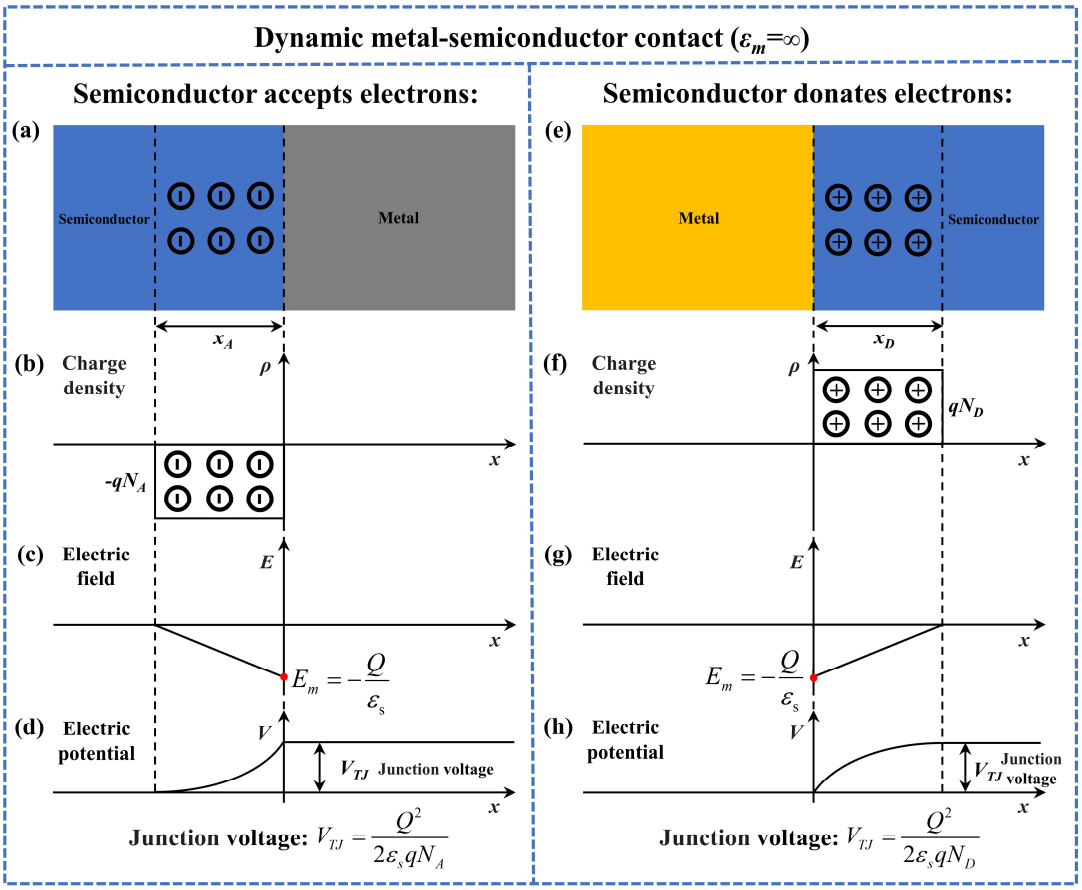

Figure S3. Formulaic analysis of the triboelectric junction in dynamic metal-semiconductor contacts. (a) Schematic diagram of the model where the semiconductor accepts electrons; and the corresponding (b) Charge density distribution; (c) Electric field distribution; (d) Electric potential distribution; (e) Schematic diagram of the model where the semiconductor donates electrons; and the corresponding (f) Charge density distribution; (g) Electric field distribution; (h) Electric potential distribution.

Standard electrode potential (Unit: V)

(-)	Mg	Al	Zn	Sn	(Si)	Cu	Ag	Pt	Au	(+)
Ions	Mg^{2+}	Al^{3+}	Zn^{2+}	Sn^{2+}	$SiH_4(g)$	Cu^{2+}	Ag^{+}	Pt^{2+}	Au^{3+}	
φ	-2.37	-1.66	-0.76	-0.13	(0.10)	0.34	0.80	1.19	1.52	

Figure S4. Standard electrode potential.

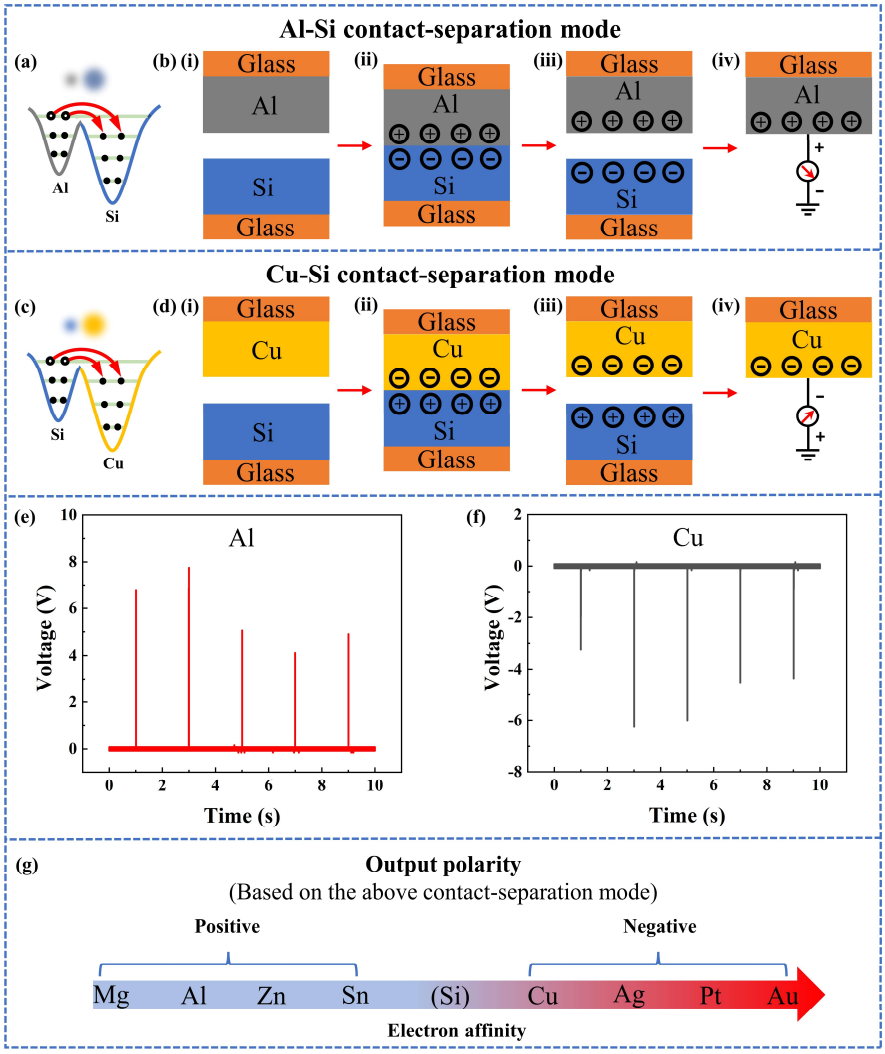

Figure S5. Verifying the relative relationship of electron affinity between various metals and silicon. (a) Schematic diagram of the electron-cloud-potential-well model and (b) Experiment for verifying the electron-affinity series between Al and Si; (c) Schematic diagram of the electron-cloud-potential-well model and (d) Experiment for verifying the electron-affinity series between Cu and Si; (e) Experiment result indicates that Al tends to donate electrons in a dynamic Al-Si contact; (f) Experiment result indicates that Cu tends to accept electrons a dynamic Cu-Si contact; (g) By utilizing the modified contact-separation-mode TENG, we can determine the output polarity of various metals after contacting with silicon. Metals with electron-affinity values smaller than Si, such as Mg, Al, Zn, and Sn, generate positive outputs. Conversely, metals with electron-affinity values larger than Si, such as Cu, Ag, Pt, and Au, generate negative outputs. Note that the Si wafers used in the modified contact-separation-mode TENG are intrinsic Si wafers with resistivity exceeding 1×10^5 Ω·cm.

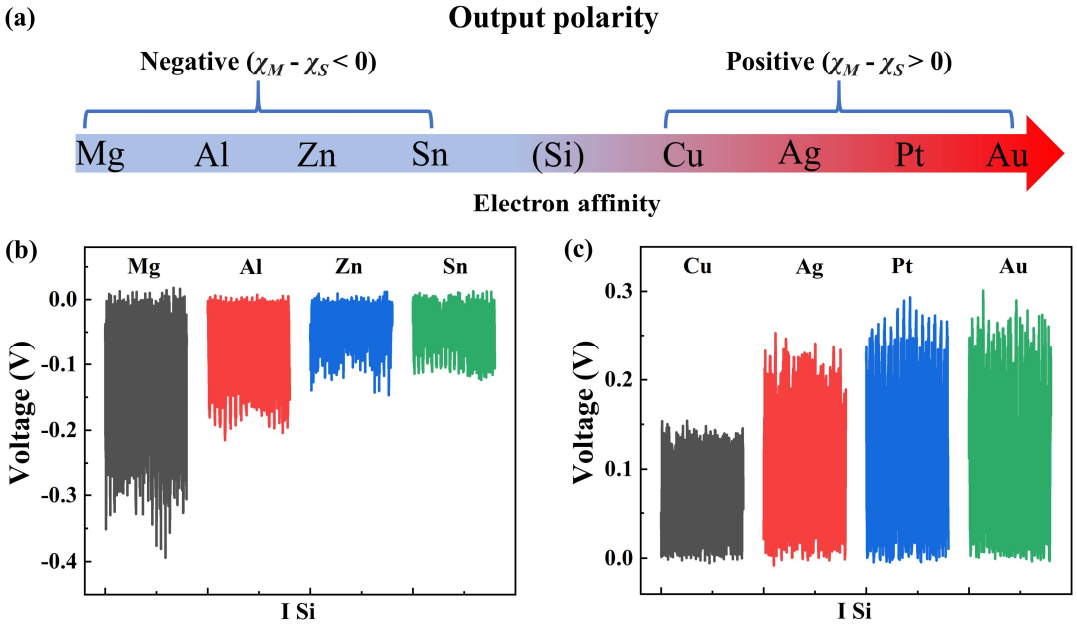

Figure S6. The junction direction determines the output polarity. (a) The sign of χ_M-χ_S indicates both the junction direction and the resulting output polarity; (b) In dynamic metal-Si contacts using metals with electron-affinity values smaller than Si, such as Mg, Al, Zn, and Sn, negative outputs are generated; (c) Conversely, in dynamic metal-Si contacts using metals with electron-affinity values larger than Si, such as Cu, Ag, Pt, and Au, positive outputs are generated.

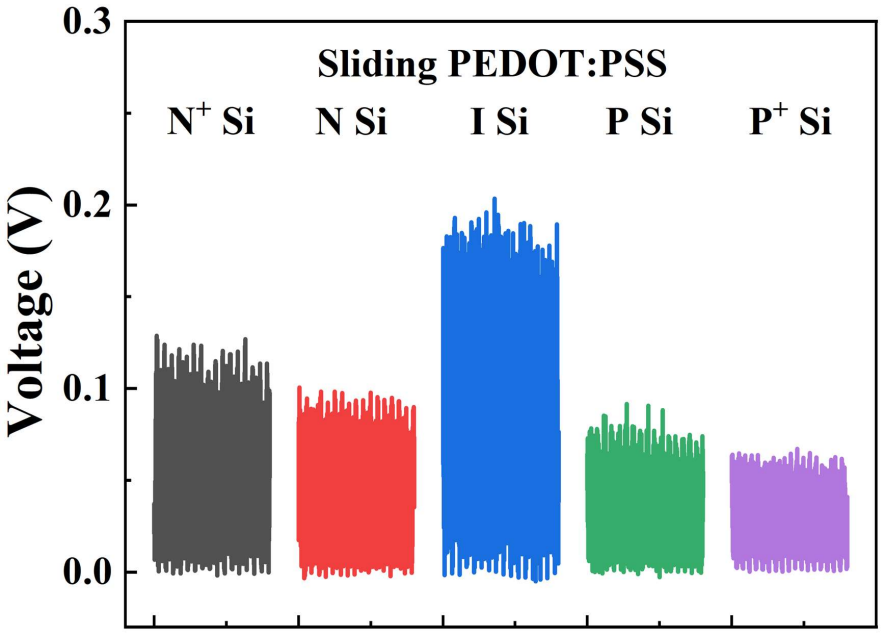

Figure S7. Existence of the triboelectric junction in dynamic semiconductor-semiconductor contacts.

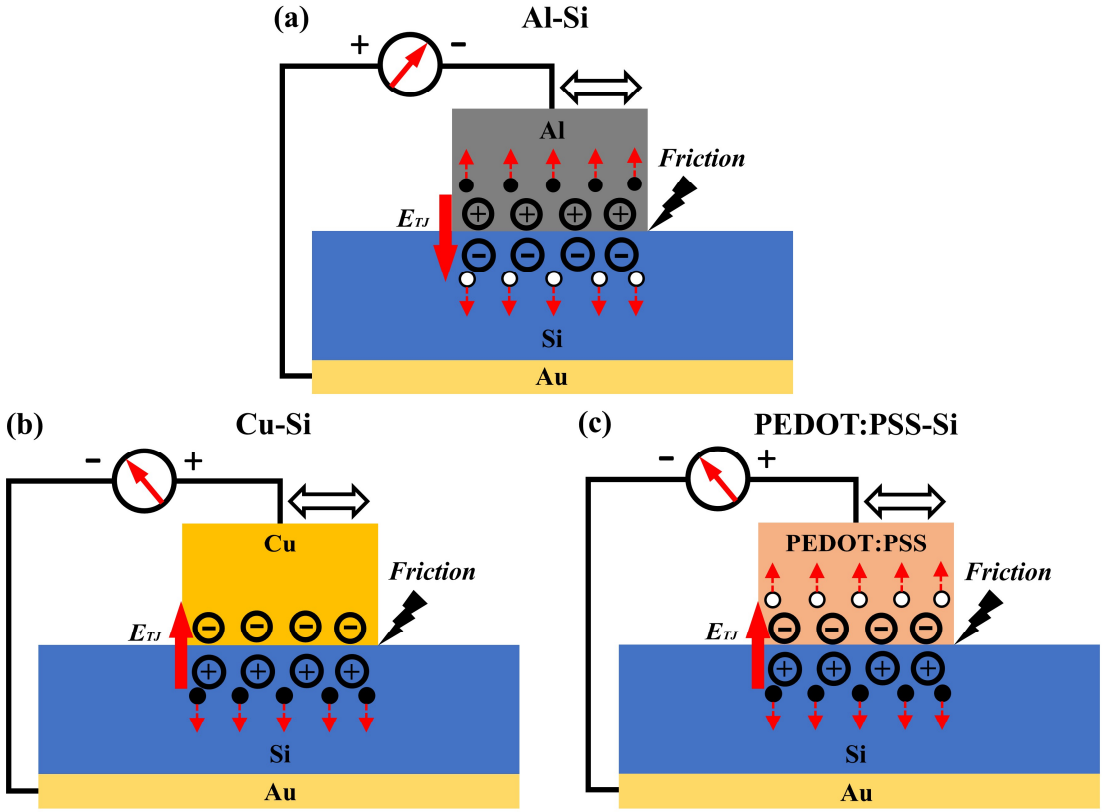

Figure S8. Working mechanism of three representative dynamic semiconductor-based contacts. (a) Dynamic Al-Si contact; (b) Dynamic Cu-Si contact, where no hole transport in Cu; (c) Dynamic PEDOT:PSS-Si contact.

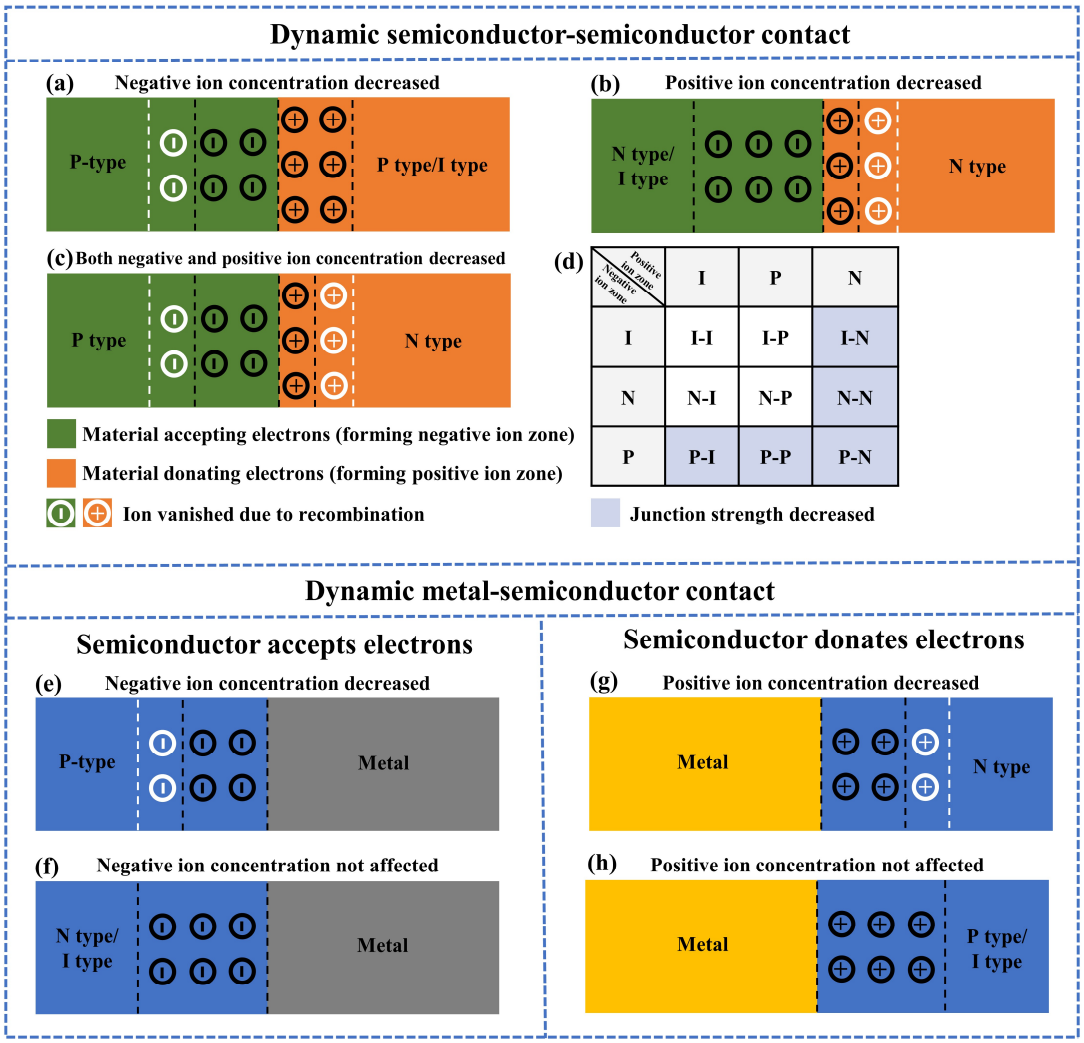

Figure S9. The influence of the Fermi level on the triboelectric junction. (a) Negative ion concentration decreased; (b) Positive ion concentration decreased; (c) Both negative and positive ion concentration decreased; (d) Various combinations of Fermi level (P-type/N-type/I-type) and ion type (positive/negative) in the triboelectric junction; (e) Negative ion concentration decreased; (f) Negative ion concentration not affected; (g) Positive ion concentration decreased; (h) Positive ion concentration not affected. Overall, when forming a negative ion zone in a P-type semiconductor, the negative ion concentration will decrease, resulting in a decrease in the junction strength. Similarly, when forming a positive ion zone in an N-type semiconductor, the positive ion concentration will decrease, resulting in a decrease in the junction strength. However, further studies are needed to determine the extent to which the Fermi level affects the triboelectric junction. Note that the analysis of the dynamic metal-semiconductor contact is considered a simplified model compared to dynamic semiconductor-semiconductor contacts.

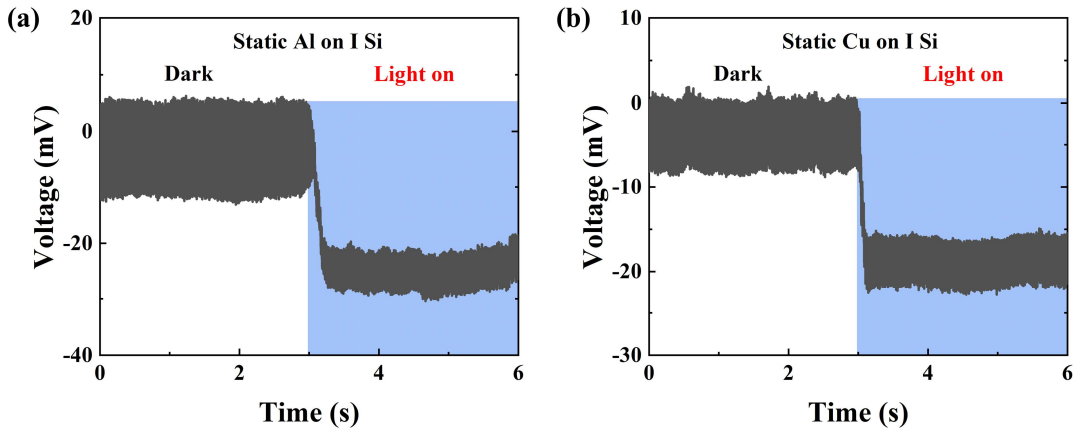

Figure S10. The photovoltaic effect in intrinsic Si-based devices. (a) The photovoltaic effect in the static contact using Al and I Si (about -25 mV under the ambient light condition in the testing lab); (b) The photovoltaic effect in the static contact using Cu and I Si (about -20 mV under the ambient light condition in the testing lab).

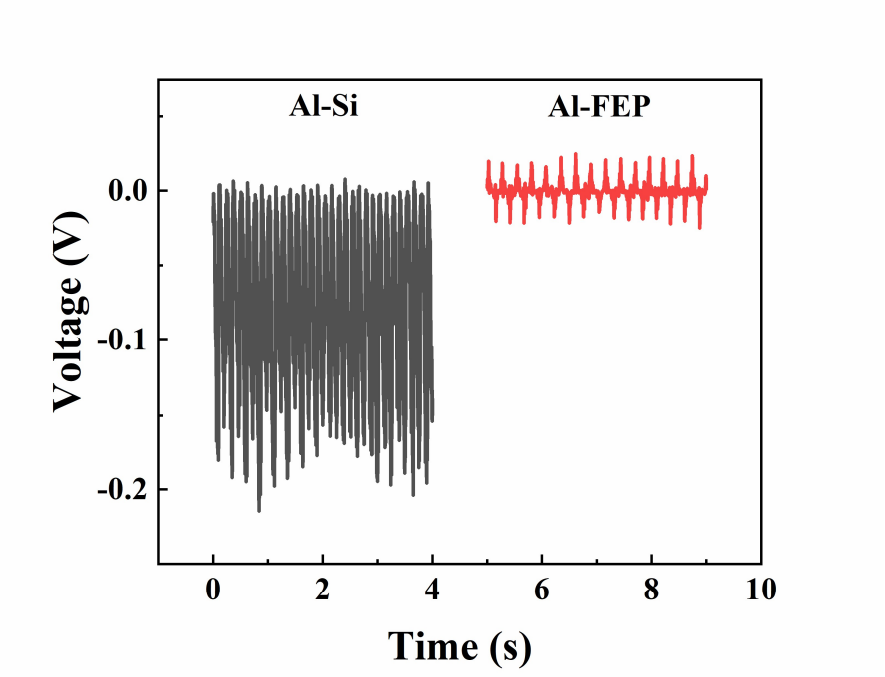

Figure S11. Comparison between dynamic metal-semiconductor and metal-insulator contacts. (a) The dynamic Al-Si contact generates direct current (unipolar output); (b) The dynamic Al-FEP contact generates alternating current (bipolar output). FEP, fluorinated ethylene propylene.

Supplementary Notes

Note S1. Detailed derivation of the formulaic analysis

A triboelectric junction is a space charge region induced by the triboelectric effect, exhibiting characteristics similar to an abrupt heterojunction. In an abrupt heterojunction, the ion types in the space charge region change abruptly from positive ions to negative ions across the contact interface. Similarly, in a triboelectric junction, one material donates electrons while the other material accepts electrons, which also presents an abrupt change in ion type. Therefore, the analysis of a triboelectric junction can be analogous to the abrupt heterojunction[3–5]. To simplify the analysis, we will discuss the triboelectric junction under a thermal equilibrium condition. In a triboelectric junction, the material that accepts (donates) electrons forms a negative (positive) ion zone with an ion concentration of N_A (N_D). The widths of the negative and positive ion zone are defined as x_A and x_D, respectively. The contact interface between the negative and positive ion zones is defined as x=0. Thus, we obtain the charge density distribution, as shown in Fig. 2b:

$$\rho(x) = \begin{cases} -qN_A, & -x_A \le x \le 0 \\ qN_D, & 0 \le x \le x_D \end{cases}. \tag{S1}$$

The width of the triboelectric junction:

$$X = x_A + x_D. \tag{S2}$$

According to the electron transfer model of the triboelectric effect[6], the space charge amount (the triboelectric charge amount) in the negative ion zone is equal to that in the positive ion zone:

$$qN_A x_A = qN_D x_D = Q, \tag{S3}$$

where Q is the space charge amount (the triboelectric charge amount) per unit area.
Equation S3 can be further simplified as

$$N_A x_A = N_D x_D. \tag{S4}$$

According to the Poisson equation[3,4], we obtain

$$-\frac{d^2V(x)}{dx^2} = \frac{dE(x)}{dx} = \frac{\rho(x)}{\varepsilon(x)} = \begin{cases} -\dfrac{qN_A}{\varepsilon_A}, & -x_A \le x \le 0 \\ \dfrac{qN_D}{\varepsilon_D}, & 0 \le x \le x_D \end{cases}. \tag{S5}$$

Integrating the above equations, we obtain

$$\frac{dV(x)}{dx} = \begin{cases} (\dfrac{qN_A}{\varepsilon_A})x + C_1, & -x_A \le x \le 0 \\ -(\dfrac{qN_D}{\varepsilon_D})x + C_2, & 0 \le x \le x_D \end{cases}, \tag{S6}$$

where C_1 and C_2 are constant, which can be derived from the boundary conditions. We discuss the triboelectric junction in a thermal equilibrium condition, in which the region outside the

triboelectric junction is electrically neutral. The electric field is concentrated in the triboelectric junction, so we obtain the boundary conditions:

$$\begin{cases} E(-x_A) = -\left.\dfrac{dV(x)}{dx}\right|_{x=-x_A} = 0 \\ E(x_D) = -\left.\dfrac{dV(x)}{dx}\right|_{x=x_D} = 0 \end{cases} . \tag{S7}$$

Substituting Equation S7 into Equation S6, we obtain

$$C_1 = \frac{qN_A x_A}{\varepsilon_A},\ C_2 = \frac{qN_D x_D}{\varepsilon_D} . \tag{S8}$$

Thus, we obtain the electric field distribution of the triboelectric junction, as shown in Fig. 2c:

$$E(x) = -\frac{dV(x)}{dx} = \begin{cases} -\dfrac{qN_A(x+x_A)}{\varepsilon_A}, & -x_A \le x \le 0 \\ \dfrac{qN_D(x-x_D)}{\varepsilon_D}, & 0 \le x \le x_D \end{cases} . \tag{S9}$$

The electric field strength is a linear function of the position x in the negative and positive ion zones, respectively. The electric field direction is from the positive ion zone to the negative ion zone, along the negative direction of the *x-axis*. At x=0, the electric field strength reaches its maximum for the negative ion zone (E_{Am}) and positive ion zone (E_{Dm}), respectively. Thus, we obtain

$$E_{Am} = -\frac{qN_A x_A}{\varepsilon_A} = -\frac{Q}{\varepsilon_A}, \tag{S10}$$

$$E_{Dm} = -\frac{qN_D x_D}{\varepsilon_D} = -\frac{Q}{\varepsilon_D} . \tag{S11}$$

Note that the electric field distribution across the contact interface (x=0) is discontinuous due to the change in the dielectric permittivity. However, the electric displacement field is continuous ($\varepsilon_A E_{Am} = \varepsilon_D E_{Dm}$).

Integrating Equation S9, we obtain the electric potential distribution:

$$V(x) = \begin{cases} (\dfrac{qN_A}{2\varepsilon_A})x^2 + (\dfrac{qN_A x_A}{\varepsilon_A})x + D_1, & -x_A \le x \le 0 \\ -(\dfrac{qN_D}{2\varepsilon_D})x^2 + (\dfrac{qN_D x_D}{\varepsilon_D})x + D_2, & 0 \le x \le x_D \end{cases} , \tag{S12}$$

where D_1 and D_2 are constants, which can be derived from the boundary conditions. Let the electric potential of the neutral region (outside the triboelectric junction) of Material A (accepting electrons) be zero. We obtain the boundary condition under thermal equilibrium condition:

$$V(-x_A) = 0,\ V(x_D) = V_{TJ} . \tag{S13}$$

Substituting Equation S13 into Equation S12, we obtain

$$D_1 = \frac{qN_A x_A^{\ 2}}{2\varepsilon_A},\ D_2 = V_{TJ} - \frac{qN_D x_D^{\ 2}}{2\varepsilon_D}. \tag{S14}$$

Substituting Equation S14 in Equation S12, we obtain the electric potential distribution:

$$V(x) = \begin{cases} \frac{qN_A(x^2 + x_A^{\ 2})}{2\varepsilon_A} + \frac{qN_A x x_A}{\varepsilon_A}, & -x_A \le x \le 0 \\ V_{TJ} - \frac{qN_D(x^2 + x_D^{\ 2})}{2\varepsilon_D} + \frac{qN_D x x_D}{\varepsilon_D}, & 0 \le x \le x_D \end{cases}. \tag{S15}$$

Note the electric potential distribution is continuous regardless of whether the electric field is continuous or not. At x=0, the electric potential is continuous:

$$V_A(0) = V_D(0)\ , \tag{S16}$$

where $V_A(x)$ and $V_D(x)$ are the electric potential distribution in the negative and positive ion zones, respectively.

Substituting Equation S16 into Equation S15, we obtain the electric potential difference across the triboelectric junction, namely the junction voltage:

$$V_{TJ} = \frac{qN_A x_A^{\ 2}}{2\varepsilon_A} + \frac{qN_D x_D^{\ 2}}{2\varepsilon_D}. \tag{S17}$$

Substituting Equation S17 into Equation S15, we obtain another expression of the electric potential distribution, as shown in Fig. 2d:

$$V(x) = \begin{cases} \frac{qN_A(x + x_A)^{\ 2}}{2\varepsilon_A}, & -x_A \le x \le 0 \\ \frac{qN_D}{\varepsilon_D}(x_D - \frac{x}{2})x + \frac{qN_A x_A^{\ 2}}{2\varepsilon_A}, & 0 \le x \le x_D \end{cases}. \tag{S18}$$

In the triboelectric junction, the electric potential distribution is parabolic in the negative and positive ion zones, respectively.

Substituting Equation S3 (qN_AX_A=qN_DX_D=Q) into Equation S17, we obtain

$$V_{TJ} = \frac{Q^2}{2\varepsilon_A qN_A} + \frac{Q^2}{2\varepsilon_D qN_D}. \tag{S19}$$

For dynamic metal-semiconductor contacts, the junction region is considered to exist solely within the semiconductor (ε_m=∞), similar to the one-sided abrupt PN junction (P^+N junction or PN^+ junction). The triboelectric junction of dynamic metal-semiconductor contacts can be divided into two categories and further simplified.

1) The semiconductor accepts electrons (see Fig. 2e, Fig. 2f, and Fig. S3):

The charge density distribution:

$$\rho(x) = -qN_A\ ,\ -x_A \le x \le 0\ . \tag{S20}$$

The electric field distribution:

$$E(x) = -\frac{dV(x)}{dx} = -\frac{qN_A(x+x_A)}{\varepsilon_A}, \quad -x_A \le x \le 0 . \tag{S21}$$

The maximum electric field strength:

$$E_m = -\frac{Q}{\varepsilon_S} . \tag{S22}$$

The electric potential distribution (Let the electric potential of the neutral region be zero):

$$V(x) = \frac{qN_A(x+x_A)^2}{2\varepsilon_A}, \quad -x_A \le x \le 0 . \tag{S23}$$

The junction voltage:

$$V_{TJ} = \frac{qN_A x_A^2}{2\varepsilon_A} = \frac{Q^2}{2\varepsilon_S q N_A} . \tag{S24}$$

2) The semiconductor donates electrons (see Fig. 2g, Fig. 2h, and Fig. S3):

The charge density distribution:

$$\rho(x) = qN_D , \quad 0 \le x \le x_D . \tag{S25}$$

The electric field distribution:

$$E(x) = -\frac{dV(x)}{dx} = \frac{qN_D(x-x_D)}{\varepsilon_D}, \quad 0 \le x \le x_D . \tag{S26}$$

The maximum electric field strength:

$$E_m = -\frac{Q}{\varepsilon_S} . \tag{S27}$$

The electric potential distribution (Let the electric potential at the contact interface be zero):

$$V(x) = \frac{qN_D}{\varepsilon_D}(x_D - \frac{x}{2})x, \quad 0 \le x \le x_D . \tag{S28}$$

The junction voltage:

$$V_{TJ} = \frac{qN_D x_D^2}{2\varepsilon_D} = \frac{Q^2}{2\varepsilon_S q N_D} . \tag{S29}$$

Although both the electric field distributions and the electric potential distributions are different between these two categories, the expression of the maximum electric field strength is the same:

$$E_m = -\frac{Q}{\varepsilon_S} . \tag{S30}$$

The junction voltage can be concluded into the same expression:

$$V_{TJ} = \frac{Q^2}{2\varepsilon_s qN} , \tag{S31}$$

where N is N_A or N_D, depending on whether the semiconductor accepts or donates electrons.

Note S2. Relationship between the open-circuit voltage and the theoretical maximum junction voltage

The junction voltage analyzed above in a thermal equilibrium condition is considered the theoretical maximum junction voltage. Note that the open-circuit voltage is closely related to, but not equal to, the junction voltage. In the context of the photovoltaic effect, the junction voltage, also known as the built-in voltage, is regarded as the upper limit of the open-circuit voltage[7,8]. When a solar cell operates in an open-circuit state, a potential difference, caused by the accumulation of charge carriers at electrodes, will partially cancel out the junction voltage[9,10]. In the case of a dynamic semiconductor generator, where non-equilibrium electron-hole generation occurs, the system is not actually in thermal equilibrium. Similar to the photovoltaic effect, the open-circuit voltage in this case would never reach the theoretical maximum junction voltage due to the accumulation of charge carriers at the electrodes. However, a larger junction voltage does contribute to a larger open-circuit voltage.

Note S3. Discussion on the parameters in the "triboelectric junction" model

From Equations S24 and S29, we can conclude the junction voltage for dynamic metal-semiconductor contacts as follows,

$$V_{TJ} = \frac{qNx^2}{2\varepsilon_S} = \frac{Q^2}{2\varepsilon_S qN} \tag{S32}$$

where N is N_A or N_D, depending on whether the semiconductor accepts or donates electrons, and x is the width of the negative or positive ion zone in the semiconductor.

Thus, we can obtain the ion concentration in the space charge region of the semiconductor,

$$N = \frac{2\varepsilon_S V_{TJ}}{qx^2} = \frac{2\varepsilon_o \varepsilon_r V_{TJ}}{qx^2} \tag{S33}$$

where ε_o and ε_r are the vacuum permittivity and relative permittivity of Si, respectively.

Note that the width of the negative or positive ion zone in the semiconductor (x), also referred to as the charge penetration depth in contact electrification, is typically less than 30 nm[11,12], and in some cases, even less than 3 nm[13]. This value can vary depending on factors such as the specific materials used, applied mechanical force, and environmental conditions.

For dynamic metal-Si contacts, by substituting $q = 1.6 \times 10^{-19}$ C, $\varepsilon_o = 8.85 \times 10^{-12}$ F/m, $\varepsilon_r = 11.9$, $V_{TJ} = 0.1$ V, and $x = 30$ nm into Equation S33, we obtain $N = 1.46 \times 10^{17}/\text{cm}^3$.

Using Equation S3, $Q = qNx$, we obtain $Q = 70.08$ nC/cm^2.

Note that the above calculations are conservative. Typically, $V_{TJ} > 0.1$ V and $x < 30$ nm. Therefore, we can conclude that $N > 1.46 \times 10^{17}/\text{cm}^3$ and $Q > 70.08$ nC/cm^2.

Note S4. A potential experimental method to examine the effect of dielectric permittivity

Based on Equation S32 (or Equation 9 in the main text), the junction voltage is influenced by the parameters Q, ε_s, and N. To investigate the effect of a single parameter, the control variable method should be employed. In the main text, we have already utilized this method to study the effect of Q. However, the approach for investigating the effect of ε_s differs.

One potential method is to use the same metal material to dynamically contact semiconductors with different dopant types and concentrations. For instance, heavily doped Si, which exhibits a higher dielectric permittivity compared to non-heavily-doped Si[14–16], can be considered. Note that the doping concentration in Si wafers is typically very low, even when they are heavily doped. In the context of Si wafers, a dopant concentration exceeding 0.1% is considered heavily doped. Hence, when heavily doped and non-heavily-doped Si dynamically contact the same metal material, the triboelectric charge density (Q) is comparable. This is because the primary atoms that come into contact at the interface are still Si atoms and metal atoms. Therefore, both Q and N can be considered comparable, while ε_s can significantly differ.

However, heavily doped Si, also known as a degenerate semiconductor, behaves more similarly to a conductor than a conventional semiconductor, which may introduce additional side effects that need to be carefully considered. Therefore, further research is required to determine an appropriate doping concentration to investigate the effect of ε_s. Additionally, exploring the doping of other semiconductor materials would also be valuable.

Supplementary Table

Table S1. Standard electrode potential table

Element	Half-reaction			$E°$ / V	Electrons
	Oxidant	⇌	Reductant		
Mg	$Mg^{2+} + 2e^-$	⇌	$Mg(s)$	-2.372	2
Al	$Al^{3+} + 3e^-$	⇌	$Al(s)$	-1.662	3
Zn	$Zn^{2+} + 2e^-$	⇌	$Zn(s)$	-0.7618	2
Sn	$Sn^{2+} + 2e^-$	⇌	$Sn(s)$	-0.13	2
Si	$Si(s) + 4H^+ + 4e^-$	⇌	$SiH_4(g)$	+0.102	4
Cu	$Cu^{2+} + 2e^-$	⇌	$Cu(s)$	0.337	2
Ag	$Ag^+ + e^-$	⇌	$Ag(s)$	0.7996	1
Pt	$Pt^{2+} + 2e^-$	⇌	$Pt(s)$	1.188	2
Au	$Au^{3+} + 3e^-$	⇌	$Au(s)$	1.52	3

Note: The data in Table S1 and Figure S4 (except for Si) are extracted from:
https://en.wikipedia.org/wiki/Standard_electrode_potential_(data_page)
The data for Si are extracted from:
https://www.av8n.com/physics/redpot.htm

Supplementary References

1 S. Lin and Z. Lin Wang, *Mater. Today*, 2023, **62**, 111–128.
2 J. Meng, C. Pan, L. Li, Z. H. Guo, F. Xu, L. Jia, Z. L. Wang and X. Pu, *Energy Environ. Sci.*, 2022, **15**, 5159–5167.
3 S. M. Sze and K. K. Ng, *Physics of Semiconductor Devices*, Wiley, 2021.
4 W. Shockley, *Bell Syst. Tech. J.*, 1949, **28**, 435–489.
5 E. Liu, B. Zhu and J. Luo, *Semiconductor Physics*, Publishing House of Electronics Industry, 2011.
6 Z. L. Wang and A. C. Wang, *Mater. Today*, 2019, **30**, 34–51.
7 Z. He, C. Zhong, X. Huang, W. Y. Wong, H. Wu, L. Chen, S. Su and Y. Cao, *Adv. Mater.*, 2011, **23**, 4636–4643.
8 J. Luo, H. Wu, C. He, A. Li, W. Yang and Y. Cao, *Appl. Phys. Lett.*, 2009, **95**, 043301.
9 B. Qi and J. Wang, *J. Mater. Chem.*, 2012, **22**, 24315–24325.
10 N. K. Elumalai and A. Uddin, *Energy Environ. Sci.*, 2016, **9**, 391–410.
11 A. F. Labadz and J. Lowell, *J. Electrostat.*, 1991, **26**, 251–260.
12 P. K. Watson and Z. Z. Yu, *J. Electrostat.*, 1997, **40**–**41**, 67–72.
13 W. J. Brennan, J. Lowell, M. C. O'Neill and M. P. W. Wilson, *J. Phys. D. Appl. Phys.*, 1992, **25**, 1513–1517.
14 S. Ristic, A. Prijic and Z. Prijic, *Serbian J. Electr. Eng.*, 2004, **1**, 237–247.
15 M. H. Andrews, A. H. Marshak and R. Shrivastava, *J. Appl. Phys.*, 1981, **52**, 6783–6787.
16 S. Dhr and A. H. Marshak, *Solid State Electron.*, 1985, **28**, 763–766.